

EXPERIMENT AND NUMERICAL SIMULATION RESULTS OF PLASMA WINDOW*

Huang Sheng, Zhu Kun¹, Shi Benliang, Lu Yuanrong, Yuan zhongxi, State Key Laboratory of Nuclear Physics and Technology, Peking University, Beijing 100871, China

Abstract

Plasma window is one of the windowless vacuum sealing techniques which can isolate high vacuum cavity from low vacuum or atmosphere device by plasma. A test bench was constructed in the past two years. In this paper, preliminary experimental results are presented and discussed. A numerical 2D FLUENT-based magneto-hydrodynamic model has been developed to investigate the sealing mechanism of plasma pressure difference distributed in plasma channel. The simulation results are consistent with the experiment results.

INTRODUCTION

Plasma window has been researched and designed as a windowless vacuum sealing technique, which can connect normal or high pressure device to a vacuum cavity with thermal plasma. As a result, it will reduce most interactions from the particles penetrating through traditional foil window. Especially, it is desired extensively in experiments using high-intensity heavy ion beams, which will break foil window in a short time, or in experiments which require mono-energy and high purity injected beams without the degrading of beam quality and foil material ionization.. Plasma window can provide an effective separation between the vacuum and atmosphere, which therefore can be a valid substitution of the traditional foil window. Plasma window was first used on electron beam welding [1] successfully, and the pressure of rough vacuum can reach 47Pa and higher vacuum degree can be obtained by more differential pumps.

In our lab, a plasma window with both 3mm and 6mm aperture was constructed. The preliminary experiment results are presented and discussed. A numerical 2D FLUENT-based magneto-hydrodynamic model has been developed to investigate the arc and flow field of plasma window. In such integral simulation model, the gas inlet segment, arc creation-developing segment and plasma gas expansion segment are all incorporated in the same model. The temperature, velocity and pressure field are presented to show the physical mechanisms for the high pressure gap within the plasma window. The simulation results have a good agreement with the experiment.

THE PLASMA WINDOW APPARATUS

The plasma window is composed by the cascaded arc approach and the differential pumping system (see Fig. 1). The cathode (X3) and anode are connected to a constant-current power supply which can deliver current up to 80A.

Noble gas, in this case Argon is fed to the plasma window arc. The arc of plasma window is restrained by the 9mm cascaded copper plates which are electrically insulated by 1mm thick boron nitride spacer plates. The total thickness and the bore radius of the cascaded plates determine the length and radius of plasma window channel respectively. Figure 2 shows the plasma window.

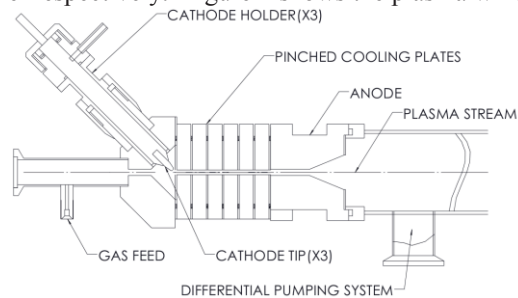


Figure 1: Diagram of plasma window.

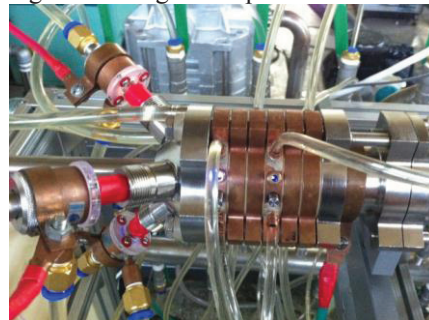


Figure 2: Photo of plasma window.

The plasma window is connected to two vacuum chambers pumped by a differential pumping system. So far, only the first chamber, the closest to the plasma window, was evacuated by an assembly of a 300L/s roots blower and a 30L/s claw-type pump.

THE PRELIMINARY TEST RESULTS

The pressure at the gas inlet of the plasma window was measured as a function of the inlet Argon flow between 0.5 and 4.2 SLM with and without arc for the aperture diameter 6mm, 6plates(i.e. channel length of 60mm). The discharge current was fixed as 62A, and the results are shown in Fig. 3. From the figure, we can find that the inlet pressure varies from 0.9KPa to 25KPa almost linearly with the increasing gas flow. The inlet pressure with 60A arc is nearly 5 times larger than which without arc.

*This work was supported by a grant from the National Natural Science Foundation of China (No. 10805003, No 91026012)

¹zhukun@pku.edu.cn

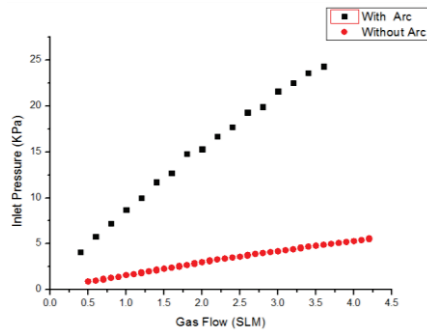


Figure 3: The inlet pressure as a function of the gas flow between with arc ($I=60A$) and without arc for aperture diameters of 6mm.

The inlet pressure was also measured as a function of the arc current for the aperture diameters between 3mm and 6mm (see Fig. 4), and for the number of cascaded plates from 3 to 6 plates (see Fig. 5) with the gas flow rate of 1.6SLM. The Fig. 4 and Fig. 5 show a linear increasing of the inlet pressure with the arc current. It is instructive that both decreasing the aperture diameter and increasing the channel length of the plasma window can help to increase the inlet pressure. But by comparing Fig. 4 with Fig. 5 we see that the effect of decreased aperture diameter is far greater than the effect of the increased length.

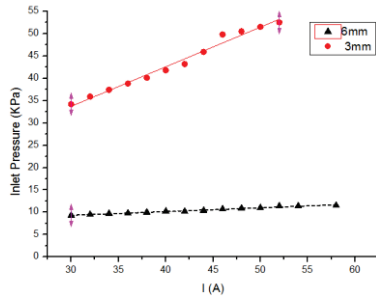


Figure 4: The inlet pressure as a function of the arc current between aperture diameters 3mm and 6mm for the gas flow rate of 1.6SLM with 6 plates.

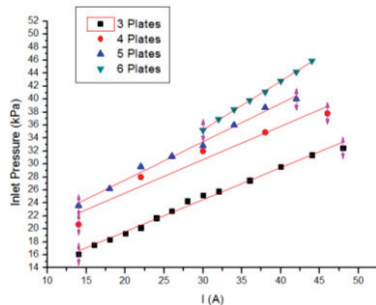


Figure 5: The inlet pressure as a function of the arc current for the number of cascaded plates from 3 to 6 plates with the gas flow rate of 1.6SL.

SIMULATION OF PLASMA WINDOW

Assumption and Basic Equations A two-dimensional axis-symmetry model for simulation of the plasma window requires solving the coupled set of nonlinear

fluid-dynamic, energy-transfer and electro-magnetic equations [2]. Further, in order to better describe the flow field inside the plasma window, turbulence phenomena are taken into account by means of a $k-\varepsilon$ model. The governing equations are as follows:

1) Mass conservation

$$\frac{\partial}{\partial z}(\rho v_z) + \frac{\partial}{\partial r}(r \rho v_r) = 0 \quad (1)$$

2) Momentum conservation

$$\frac{\partial}{\partial z}(\rho v_z v_z) + \frac{1}{r} \frac{\partial}{\partial r}(r \rho v_r v_r) = -\frac{\partial P}{\partial z} + 2 \frac{\partial}{\partial z} \left(\mu \frac{\partial v_z}{\partial z} \right) \quad (2)$$

$$+ \frac{1}{r} \frac{\partial}{\partial r} \left[r \mu \left(\frac{\partial v_r}{\partial z} + \frac{\partial v_z}{\partial r} \right) \right] + j_r B_\theta$$

$$\frac{\partial}{\partial z}(\rho v_z v_r) + \frac{1}{r} \frac{\partial}{\partial r}(r \rho v_r v_r) = -\frac{\partial P}{\partial r} + \frac{2}{r} \frac{\partial}{\partial z} \left(r \mu \frac{\partial v_r}{\partial r} \right) \quad (3)$$

$$+ \frac{\partial}{\partial r} \left[\mu \left(\frac{\partial v_z}{\partial r} + \frac{\partial v_r}{\partial z} \right) \right] - 2 \mu \frac{v_r}{r^2} - j_z B_\theta$$

3) Energy conservation

$$\frac{\partial}{\partial z}(\rho v_z h) + \frac{1}{r} \frac{\partial}{\partial r}(r \rho v_r h) = \frac{\partial}{\partial z} \left(\frac{k}{C_p} \frac{\partial h}{\partial z} \right) \quad (4)$$

$$+ \frac{1}{r} \frac{\partial}{\partial r} \left(r \frac{k}{C_p} \frac{\partial h}{\partial r} \right) + \frac{j_r^2 + j_z^2}{\sigma} + \frac{5}{2} \frac{k_B}{e} \vec{j} \cdot \nabla T - q_r$$

The radiation cooling, which is integrated into the source term of the energy equation, is described by the following equation,

$$q_r = \nabla \cdot \overline{q_{rad}} = 4\pi \varepsilon_N \quad (5)$$

where ε_N means the net emission coefficients varying with temperature [3].

4) Ohm's law and electric potential equation

$$j_z = -\sigma \frac{\partial \phi}{\partial z} \quad (6)$$

$$j_r = -\sigma \frac{\partial \phi}{\partial r} \quad (7)$$

$$\frac{\partial}{\partial z} \left(\sigma \frac{\partial \phi}{\partial z} \right) + \frac{1}{r} \frac{\partial}{\partial r} \left(\sigma r \frac{\partial \phi}{\partial r} \right) = 0 \quad (8)$$

5) Vector potential equation for magnetic field

$$\nabla^2 A_z = -\mu_0 j_z \quad (9)$$

$$\nabla^2 A_r = -\mu_0 j_r \quad (10)$$

$$B_\theta = -\frac{\partial A_z}{\partial r} + \frac{\partial A_r}{\partial z} \quad (11)$$

where μ_0 is the permeability of free space with the assumption of no ferro-magnetic material in the domain.

The equations (1)-(11) are constructed on the following assumptions:

- The plasma flow in plasma window is steady, continuous, axisymmetric and optically thin;
- The plasma is assumed to be in local thermodynamic equilibrium (LTE) state and electrically neutral;
- The thermodynamic and transport properties of the argon plasma are functions of the plasma temperature and pressure from the literature [4].

Simulation Results and Discussion The model of the plasma window, is running for $I=47A$, the inlet and outlet stagnant pressure of 52.5KPa and 60Pa respectively. Such

as the current density profile and the temperature profile which are shown in Figs. 6-8 are discussed to analyze the behavior and mechanism of the plasma window.

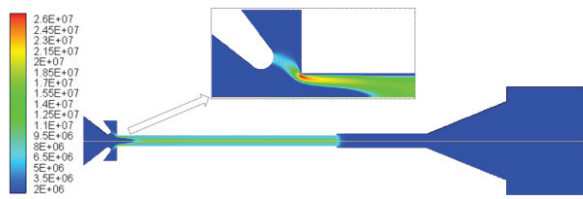


Figure 6: Computed current distribution within the plasma window.

Figure 6 shows the current distribution in cathode zone of plasma window. It can be seen that the arc at the discharge chamber is compressed along the cooling wall by the injected cold argon gas. As a result a cold gas well forms at the beginning part of plasma channel, where the cold air is gradually discharged and heated up to 10^4 K, and then the arc starts to fill the channel completely and fully developed. As the total current is a constant, the current density along the well wall is much higher than the current density of the fully developed arc. At the region near the cathode, it is also found that the arc root is flowed to the leeside of the cathode tip. The current density becomes comparatively very low as the volume increases dramatically as the radius is bigger.

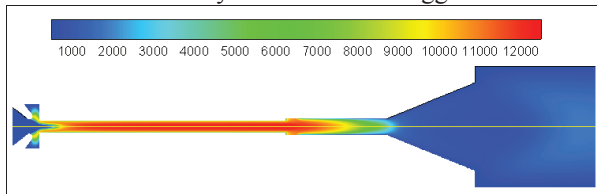


Figure 7: Computed temperature distribution within the plasma window.

The predicted temperature distribution within the plasma window is plotted in Fig. 7. The variation of pressure and velocity along the plasma window axis are further plotted in Fig. 8. It is seen that high temperature appears in the downstream region along the axis of the plasma window, with the highest temperature of 12500K and average of 10233K.

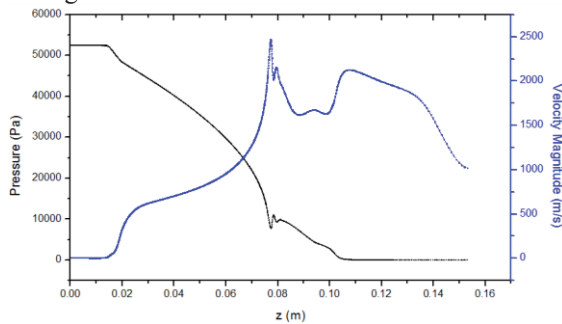


Figure 8: Computed velocity and pressure distribution along the plasma window axis.

The incoming gas flow and pumping rate was determined from the simulation itself, and have a good agreement with the experiment results as shown in Table

1. The actual cathode potential is greatly affected by the none-LTE plasma at the regions near the electrodes, where the conductivity is much higher than the LTE model as in our case. And this is the main reason that the computed potential is quite larger than the experiment result.

Table 1: Comparison of the Cathode Potential, Gas Flow and Pumping Rate between Experiment and Simulation Results

	Inlet Pressure	Outlet Pressure	I	ϕ	Gas Flow
Experiment	52.5KPa	60Pa	47A	115V	4.87E-5kg/s
Computed	Fixed	Fixed	Fixed	140V	5.12E-5kg/s
Error				17.8%	4.8%

CONCLUSIONS

Plasma window with different discharge channel diameters and lengths were experimentally investigated as a function of the operational parameters such as gas flow and current. Higher current and gas flow will help to increase the sealing ability of plasma window almost linearly. The aperture diameter plays a much more important factor than the channel length does. From the simulation, the temperature distribution shows that an average temperature of 10200K in the domain can be attained at 47A and 140V. From the pressure, temperature and velocity distribution within the plasma window, it can be inspected that the pressure drop window is very complicated which interacts with both the temperature and velocity field and is closely related with the shape of the flow tunnel. The simulated results of gas flow and cathode potential agree with experiment results. The validity of the numerical simulation model is hopeful to provide a more convenient and cheaper method to research the characterization of plasma window.

ACKNOWLEDGMENTS

This research has been supported by the National Natural Science Foundation of China (No. 10805003, No 9102601). The authors especially thank Ady Hershcovitch from Brookhaven National Laboratory and Yang Lei from Chinese Academy of Science for their help in our experiment and simulation work.

REFERENCES

- [1] A. Hershcovitch, High pressure arcs as vacuum atmosphere interface and plasma lens for nonvacuum electron beam welding machines, *Journal of Applied Physics*, 78 (1995) 1.
- [2] S. Huang, K. Zhu, B. Shi, Y. Lu, Simulation of Plasma Window for Gas Target of Neutron Source, *Proceedings of IPAC2012, New Orleans, Louisiana, USA*, (2012).
- [3] J. Menart, S. Malik, Net emission coefficients for argon-iron thermal plasmas, *JOURNAL OF PHYSICS D: APPLIED PHYSICS*, 35 (2002) 867-874.
- [4] A.B. Murphy, C.J. Arundelli, Transport coefficients of argon, nitrogen, oxygen, argon-nitrogen, and argon-oxygen plasmas, *Plasma Chem Plasma Process*, 14 (1994) 451-490.